Numerical simulation of a single oriented mini-pipe for electronic cooling systems

César Manuel Valencia-Castillo[1*], Giuseppe Zummo[2], Luca Saraceno[2], Felipe Noh-Pat[3], Pedro Cruz-Alcántar[4], Rocío Lizeth Hernández-Flores[1]

[1]*UAMRHS, Autonomous University of San Luis Potosí, 79960, Tamazunchale, Mexico*
[2]*Energy Technologies Department, ENEA, 00123, Rome, Italy*

[3]*Faculty of Engineering, Autonomous University of Campeche, 24085, Campeche, Mexico*
[4]*UAMRA, Autonomous University of San Luis Potosí, 78700, Matehuala, Mexico*

Fecha de recepción: 19 de enero de 2026 - Fecha de aceptación: 11 de mayo de 2026

Abstract

Mini-pipes are critical components in electronic cooling systems, necessitating precise design to enhance thermal performance. Within these pipes, liquid or two-phase flow circulate through oriented paths. Numerical simulation is essential for improving the design. This paper presents an own algorithm that, based on a one-dimensional steady-state model, enables the calculation of key performance parameters for single-oriented mini-tube in electronic cooling applications. A comprehensive parametric analysis, using a single oriented mini-tube with R1336mzz(Z) as the working fluid, demonstrates the algorithm's utility. The analysis yields valuable insights into the interplay between design parameters and system performance. Results indicate that the superior performance is achieved by maximizing the inner tube diameter and minimizing the tube slope. Furthermore, this algorithm serves as a valuable tool for simulating micro-scale cooling systems, allowing for design refinement and performance prediction prior to the development of experimental facilities.

Keywords: Mini-pipe, electronic cooling system, liquid flow, two-phase flow.

Simulación numérica de un mini-tubo orientado para sistemas de enfriamiento en electrónica

Resumen

Los mini-tubos son componentes críticos en los sistemas de enfriamiento para electrónica, requiriendo diseño preciso para mejorar el desempeño térmico. Dentro de estos tubos, flujo líquido o bifásico circula a través de trayectorias orientadas. La simulación numérica es esencial para la mejora del diseño. Este artículo presenta un algoritmo propio que, basado en un modelo unidimensional en estado estacionario, permite el cálculo de parámetros claves de funcionamiento para un mini-tubo orientado con R1336mzz(Z) como el fluido de trabajo, demostrando la utilidad

*cesar.valencia@uaslp.mx

Nota: Este artículo de investigación es parte de Ingeniería–Revista Académica de la Facultad de Ingeniería, Universidad Autónoma de Yucatán, Vol. 30, No. 2, 2026, ISSN: 2448-8364.

del algoritmo. El análisis proporciona información valiosa de la relación entre los parámetros de diseño y el funcionamiento del sistema. Los resultados indican que el rendimiento superior se alcanza al maximizar el diámetro interno del tubo y al minimizar la inclinación del tubo. Más aún, este algoritmo sirve como herramienta valiosa para la simulación de sistemas de enfriamiento en micro-escala, permitiendo la mejora del diseño y la predicción del funcionamiento antes del desarrollo de instalaciones experimentales.

Palabras clave: Mini-tubo, sistemas de enfriamiento en electrónica, flujo líquido, flujo bifásico.

Nomenclature

Symbol	Description	SI unit	Symbol	Description	SI unit
Roman			**Greek**		
A	Cross sectional area	m^2	Δp	Pressure drop	Pa
c_p	Specific heat capacity	$J \cdot kg^{-1} \cdot K^{-1}$	ΔT	Temperature difference	K
$\mathrm{d}z$	Differential axial length	m	Δx	Mass quality difference	$-$
D	Inner tube diameter	m	ε	Void fraction	$-$
f	Fanning friction factor	$-$	μ	Dynamic viscosity	$Pa \cdot s$
g	Gravitational acceleration	$m \cdot s^{-2}$	ρ	Density	$kg \cdot m^{-3}$
G	Mass flux	$kg \cdot m^{-2} \cdot s^{-1}$	$\dot{\sigma}$	Rate of entropy production	$W \cdot K^{-1}$
i	Specific enthalpy	$J \cdot kg^{-1}$	$\emptyset$	Two-phase multiplier	$-$
L	Axial length	m	Ω	Tube orientation	$^\circ$
$\dot{m}$	Mass flow rate	$kg \cdot s^{-1}$	**Subscripts**		
p	Pressure	Pa	e	Exit of differential length $\mathrm{d}z$	
Re	Reynolds number	$-$	f	Frictional	
s	Specific entropy	$J \cdot kg^{-1} \cdot K^{-1}$	g	Gravitational head	
T	Temperature	$^\circ C$	h	Hydrodynamic entrance	
u	Axial velocity	$m \cdot s^{-1}$	H	Hydraulic	
$\dot{W}$	Power	W	i	Inlet of differential length $\mathrm{d}z$	
x	Mass quality	$-$	in	Tube inlet	
X	Martinelli parameter	$-$	L	Liquid phase	
z	Axial distance from the inlet	m	out	Tube outlet	
z^+	Dimensionless length	$-$	sat	Saturated	
			V	Vapor phase	

1. Introduction

The current trend of miniaturization and increased power density in electronics has generated critical thermal management challenges. Given the severely limited space, the meticulous and optimized design of effective cooling systems is paramount. A refrigeration circuit, as cooling system, seems to be a good solution. Despite research advancements in recent years, some critical aspects remain unclear [1].

In a refrigeration circuit, several components work together. One of these is the piping, which connects the main components, such as the evaporator, condenser, and pump. Within these pipes, which are generally circular in cross-section, the fluid can circulate in liquid flow or in two-phase flow. The design of piping is especially important, as it influences the overall efficiency of the cooling system.

Reviews of various topics have been developed. Saisorn and Wongwises [2] conducted a literature review of research on two-phase flow in microchannels, addressing topics such as micro hydrodynamics related to the characteristics of two-phase adiabatic flow in circular and non-circular microchannels. Xu et al. [3] performed a comprehensive analysis of correlations and experimental investigations of two-phase friction pressure drop, having founded that two correlations offer the most favorable predictions. Santra et al. [4] provide a review of the numerical modeling of multiphase and multicomponent flows in microfluidic systems using the phase field method. Wörner [5] presented a review of numerical methods and models for simulations of multiphase flows.

Theoretical, numerical, and experimental analysis show interesting results. Xiao et al. [6] developed a mechanistic model for two-phase gas-liquid flow in horizontal and near-horizontal pipelines, claiming that the proposed model offers greater precision than the reviewed correlations. Parlak et al. [7] conducted a study based on the second law of thermodynamics to examine the steady, laminar flow of water in adiabatic microtubes, founding that the flow behavior in smooth microtubes differs significantly from that observed in larger-diameter tubes with respect to viscous heating, total entropy generation, and lost work. Celata et al. [8] conducted an experimental investigation to define the diabatic behavior of single-phase laminar flow in circular micro-ducts, founding that reducing the microtube diameter results in a decrease in the Nusselt number, axial dependence due to entrance effects. Zhuo et al. [9] conducted experimental and numerical studies to analyze the laminar flow and heat transfer characteristics of a liquid within smooth and rough microtubes, showing that the friction factor in the smooth microtubes was accurately predicted by conventional theory, while in the rough microtubes it was higher and increased with roughness. Sahar et al. [10] conducted a numerical study of the two-phase liquid-vapor flow using the VOF method, showing satisfactory agreement with experimental observations. Ghorai and Nigam [11] performed two-phase CFD simulations to study the behavior of gas-liquid flow in pipes, observing good agreement between the comparison of experimental and computational profiles.

Effects of properties and dimensionless numbers have been explored. Koo and Kleinstreuer [12] explored the effects of viscous dissipation on temperature distribution and friction factor in microducts using dimensional analysis and experimentally validated computer simulations. Chinnov and Kabov [13] conducted an analysis of two-phase flow patterns in capillary channels, corroborating that thermocapillary effects can be relevant under non-isothermal two-phase flow conditions in microchannels and under conditions of weak gravitational effect. Brauner and Ulmann [14] discussed flow pattern maps in adiabatic mini and micro tubes in gas-liquid systems, accounting the effects of the Eotvos number.

This paper presents an own algorithm that, based on a one-dimensional steady-state model, permits to compute key parameters of a single oriented mini-tube for electronic cooling. A comprehensive parametric analysis, utilizing a single oriented mini-tube with R1336mzz(Z) as the working fluid, is presented as example of the use of such algorithm. The fluid can be liquid or two-phase (liquid-vapor). This detailed investigation provides valuable insights into the relationships between design parameters (inner tube diameter and orientation)) and system performance (hydraulic pumping power, entropy production, and temperature and mas quality differences).

Furthermore, this algorithm should offer valuable information for thermal engineers on the feasible design and development of new loops for cooling systems applied in electronic devices, as well as to reduce the analysis time and the production cost before these can be manufactured. In addition, it can serve as a useful tool to perform numerical simulations for cooling micro-systems before setting up an experimental facility.

2. Methodology

The system under study is a single circular tube, through which liquid or two-phase (liquid-vapor) flows. Figure 1 presents a schematic of the system. The key components and characteristics are as follows. The single tube consists of a smooth oriented circular tube, with an inner tube diameter, D, and a total length, L, oriented at an angle, Ω, from the horizontal. The entire tube is thermally isolated. The fluid enters at the tube "inlet" with constant mass flux, G, at the inlet temperature, T_{in}; and, for the case of subcooled liquid flow, at the inlet pressure, p_{in}, while for the case of two-phase flow, at the inlet quality, x_{in}. It is important to highlight that the fluid at the inlet is considered as subcooled liquid ($p_{in} > p_{sat}(T_{in})$), or saturated two-phase ($0 < x_{in} < 1$). Subsequently, the fluid flows along the tube, whose length is L, losing pressure. For the case of two-phase flow, liquid and vapor phases are present in equilibrium. Finally, the fluid exits at the tube "outlet". The z-axis is chosen to be along the tube, beginning at the tube inlet. For the simulation, the fluid, through the total length, L, enters at the differential inlet, i, and exit at the differential exit, e, having traveled the differential length, dz.

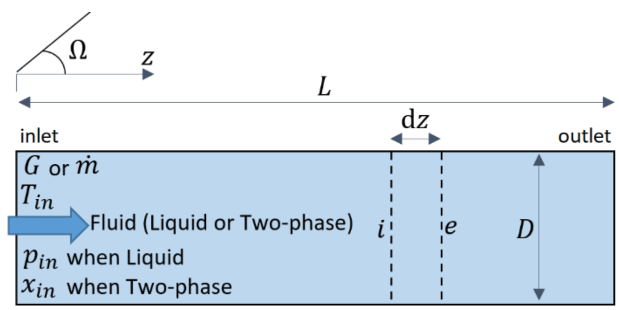

Figure 1. Schematic of the tube.

For the analysis and simulation, the following considerations are assumed:

1) Steady-state condition.
2) One-dimensional (axial) condition.
3) Thermally isolated tube.
4) Liquid and vapor, for the two-phase flow, are in thermodynamic equilibrium along the differential length, dz.
5) Constant properties and parameters along the differential axial length, dz.
6) The inner surface of the tube is smooth.

Figure 2 illustrates the flow chart of the algorithm developed to simulate the system. The algorithm has been implemented in Python software [15].

The algorithm requires several input parameters to simulate the system. These parameters are the inner tube diameter, D, the axial length, L, the tube orientation, Ω, the mass flux, G, or the mass flow rate, $\dot{m}$, the inlet temperature, T_{in}, the inlet pressure (for liquid flow), p_{in}, or the inlet mass quality (for two-phase flow), x_{in}, and the differential axial length, dz.

The liquid flow and two-phase flow routines are described in subsequent sections.

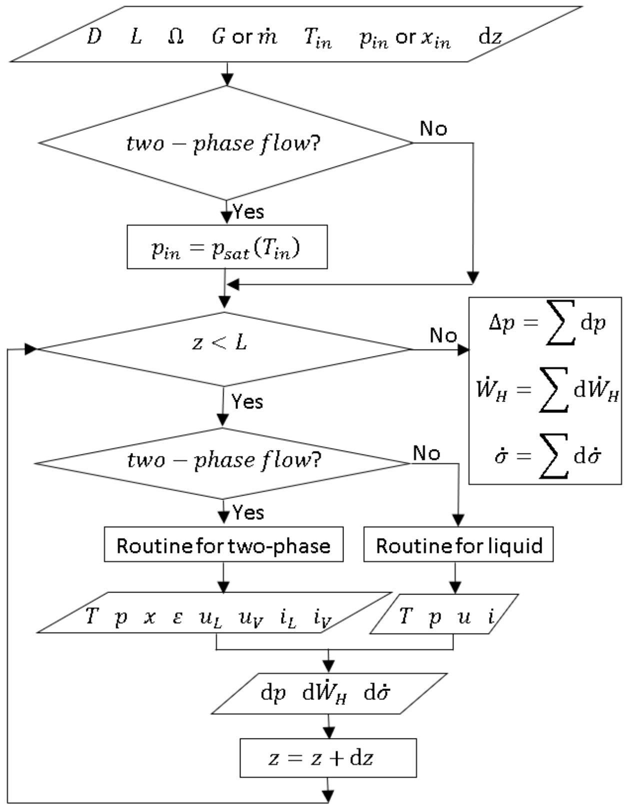

Figure 2. Flow chart of the present algorithm.

2.1. Liquid flow

For the present analysis, the inlet pressure must be greater than the saturation pressure at the inlet temperature ($p_{in} > p_{sat}(T_{in})$) to ensure that the fluid enters the tube as subcooled liquid.

Total pressure drop is a parameter that includes head and frictional effects.

The head pressure drop, $\mathrm{d}p_g$, has been estimated according to:

$$\frac{\mathrm{d}p_g}{\mathrm{d}z} = \rho g \sin\Omega \quad (1)$$

The frictional pressure drop, $\mathrm{d}p_f$, has been estimated according to:

$$\frac{\mathrm{d}p_f}{\mathrm{d}z} = \frac{2f\rho u^2}{D} \quad (2)$$

Where f is the Fanning friction factor.

The frictional effects depend on the flow regime.

For laminar flow, the flow could be hydrodynamic developing or fully-developed. The criterion of the beginning of hydrodynamic fully-developed laminar flow is the hydrodynamic entrance length, L_h, which has been estimated by the well-accepted equation $L_h = 0.05DRe$.

For hydrodynamic developing laminar flow, the Fanning friction factor, f, for circular channels, has been estimated according to Shah and London [16] as:

$$f = \left[C_1 + \frac{C_2 - C_1}{C_3}\right]\frac{D}{4L} \quad (3)$$

Where $C_1 = 13.74(z^+)^{0.5}$, $C_2 = 1.25 + 64z^+$, and $C_3 = 1 + 0.00021(z^+)^{-2}$. The dimensionless length z^+ is defined as $z^+ = (L/D)Re^{-1}$

For hydrodynamic fully-developed laminar flow, the Fanning friction factor, f, for circular channels is estimated by equation:

$$f = 16Re^{-1} \quad (4)$$

For turbulent flow, Phillips [17] presented equation to cover both, the developing and fully-developed flow regions.

$$f = CRe^{-n} \tag{5}$$

Where $C = 0.0929 + 1.01612(D/L)$ and $n = 0.268 + 0.3293(D/L)$.

So, the total pressure drop, $\mathrm{d}p$, includes gravitational head and frictional and effects.

$$\frac{\mathrm{d}p}{\mathrm{d}z} = \frac{\mathrm{d}p_g}{\mathrm{d}z} + \frac{\mathrm{d}p_f}{\mathrm{d}z} \tag{6}$$

So, the pressure at the exit "e", p_e, of the differential length, $\mathrm{d}z$, is:

$$p_e = p_i + \mathrm{d}p \tag{7}$$

Where p_i is the pressure at the inlet "i" of the differential length $\mathrm{d}z$.

Now, it is necessary to know a second independent intensive property at the exit, e.

The rate of entropy production due to frictional pressure drop is estimated, according to Bejan [18], with the following equation:

$$\frac{\mathrm{d}\dot{\sigma}}{\mathrm{d}z} = \frac{32\dot{m}^3 f}{\pi^2\rho^2 T D^5} \tag{8}$$

The mass flow rate, $\dot{m}$, is estimated according to $\dot{m} = GA$, where A is the cross-sectional area.

According with an entropy balance, the specific entropy at the exit, s_e, could be obtained as:

$$s_e = s_i + \frac{\mathrm{d}\dot{\sigma}}{\dot{m}} \tag{9}$$

Where s_i is the specific entropy at the inlet.

So, it is possible to compute the rest of properties at the exit, e, as function of the pressure and the specific entropy; for example, the temperature, $T_e(p_e, s_e)$.

To estimate the hydraulic pumping power, the following equation has been used:

$$\mathrm{d}\dot{W}_H = \frac{\dot{m}}{\rho}\mathrm{d}p \tag{10}$$

2.2. Two-phase flow

For the case of two-phase (liquid-vapor) flow, the gravitational head pressure drop has been computed according to equation 1, where the two-phase density is estimated as $\rho = (1-x)\rho_L + x\rho_V$.

The frictional pressure drop is estimated as [19]:

$$\frac{\mathrm{d}p_f}{\mathrm{d}z} = \phi_L^2 \frac{\mathrm{d}p_{f,L}}{\mathrm{d}z} \tag{11}$$

Where ϕ is called the two-phase multiplier. According with Lockhart and Martinelli [20], such multiplier, for liquid phase, is computed as:

$$\phi_L = \left(1 + \frac{C}{X} + \frac{1}{X^2}\right)^{1/2} \tag{12}$$

Where C is a constant depending on the flow regime of the phases, and X is the Martinelli parameter. Table 1 shows the values of C for the four possible combinations.

Table 1. Constant value to compute the two-phase multiplier.

Liquid	Vapor	C
Turbulent	Turbulent	20
Laminar	Turbulent	12
Turbulent	Laminar	10
Laminar	Laminar	5

The Martinelli parameter is defined as [19]:

$$X = \left(\frac{\mathrm{d}p_{f,L}/\mathrm{d}z}{\mathrm{d}p_{f,V}/\mathrm{d}z}\right)^{1/2} \tag{13}$$

The frictional pressure drop, $\mathrm{d}p_f$, for each phase, has been estimated according to [19]:

$$\frac{\mathrm{d}p_{f,L}}{\mathrm{d}z} = \frac{2f_L G_L^2}{\rho_L D} \quad ; \quad \frac{\mathrm{d}p_{f,V}}{\mathrm{d}z} = \frac{2f_V G_V^2}{\rho_V D} \tag{14}$$

Where the mass fluxes of the phases

estimated as $G_L = (1-x)G$ and $G_V = xG$.

The Fanning friction factor, f, for each phase has been estimated according to [19]:

$$f_L = CRe_L^{-n} \quad ; \quad f_V = CRe_V^{-n} \tag{15}$$

Where C and n are 16 and 1, respectively, for laminar flow, and 0.079 and 0.25, respectively, for turbulent flow.

Reynolds number for each phase are calculated as [19]:

$$Re_L = \frac{u_L \rho_L D_L}{\mu_L} \; ; \; Re_V = \frac{u_V \rho_V D_V}{\mu_V} \tag{16}$$

Where the individual mean phase velocities have been computed as [19]:

$$u_L = \frac{G_L}{(1-\varepsilon)\rho_L} \quad ; \quad u_V = \frac{G_V}{\varepsilon \rho_V} \tag{17}$$

Where ε is the void fraction, defined as $\varepsilon = A_V/A$.

The diameters, of each phase, are $D_L = (1-\varepsilon)D$ and $D_V = \varepsilon D$. The total pressure drop, $\mathrm{d}p$, has been computed according to equation 6. So, the pressure at the exit "e", p_e, of the differential length, $\mathrm{d}z$, is estimated according to equation 7.

The local temperature is the saturation temperature at the local pressure, p_e, i.e., $T_e = T_{sat}(p_e)$.

Now, it is necessary to know a second independent intensive property. The rate of entropy production due to frictional pressure drop, for each phase, is estimated with the following equations [18]:

$$\frac{\mathrm{d}\dot{\sigma}_L}{\mathrm{d}z} = \frac{32\dot{m}_L^3 f_L}{\pi^2 \rho_L^2 T D^5} \quad \frac{\mathrm{d}\dot{\sigma}_V}{\mathrm{d}z} = \frac{32\dot{m}_V^3 f_V}{\pi^2 \rho_V^2 T D^5} \tag{18}$$

Where $\dot{m}_L = (1-x)\dot{m}$ and $\dot{m}_V = x\dot{m}$.

The entropy production, per mass unit, and along the differential length, $\mathrm{d}z$, of the two-phase flow is:

$$\frac{\mathrm{d}\dot{\sigma}}{\dot{m}} = \frac{\mathrm{d}\dot{\sigma}_L}{\dot{m}_L} + \frac{\mathrm{d}\dot{\sigma}_V}{\dot{m}_V} \tag{19}$$

According with an entropy balance, the specific entropy at the exit, s_e, could be obtained as equation 9.

So, it is possible to compute the rest of properties at the exit, e, as function of the pressure and the specific entropy; for example, the mass quality, $x_e(p_e, s_e)$.

To estimate the hydraulic pumping power, the following equation has been used:

$$\mathrm{d}\dot{W}_H = \left(\frac{\dot{m}_L}{\rho_L} + \frac{\dot{m}_V}{\rho_V}\right)\mathrm{d}p \tag{20}$$

2.3. Working fluid

For the present analysis, the fluid R1336mzz(Z) has been selected as working fluid. This fluid may be used as an alternative refrigerant in R245FA, and it is considered to be a high temperature heat pump or the like in the future. The refrigerant is extremely safe because it is not flammable or toxic [21].

The properties of the working fluid have been computed using the REFPROP 10 software package [22]. The main properties of this refrigerant are presented in Table 2.

Table 2. Properties of R1336mzz(Z) at 1 atm.

Property	Value	Unit
T_{sat}	33.4	$°C$
i_{LV}	164.5	$kJ \cdot kg^{-1}$
$\rho(20°C)$	1,377.7	$kg \cdot m^{-3}$
$\mu(20°C)$	0.3858x10^{-3}	$Pa \cdot s$
$c_p(20°C)$	1,210.3	$J \cdot kg^{-1} \cdot K^{-1}$

3. Results and discussion

Table 3 shows the input parameters for the analyzed system. For the case of liquid flow, $p_{in} = 2\ bar$ has been set, while $x_{in} = 0.3$ has been set for the case of two-phase flow. The input parameters have been set in 27 cases combining 3 inner tube diameters and 9 tube orientations. Each of these cases have been simulated for liquid and two-phase flow.

Table 3. Input parameters for the simulation.

Parameter	Value	Unit
L	500	mm
D	$4, 6, 8$	mm
Ω	$0-90$	$°$
$\dot{m}$	10	$kg \cdot h^{-1}$
T_{in}	50	$°C$
p_{in}	2	bar
x_{in}	0.3	$-$
dz	0.1	mm

Figure 3 depicts the effect of the tube orientation, Ω, on the total pressure drop per unit of length, $\Delta p/L$, for different inner tube diameter, D.

The higher slope, the higher pressure drop, because the head gravitational increases. The smaller inner tube diameter, the higher pressure drop, because the frictional effects are higher. In liquid flow this effect is almost zero because the dominant effect is the head gravitational effect. For the case of two-phase flow, the effect of the diameter on the pressure drop is significative for $4\ mm$ on 6 and $8\ mm$; for example, for the case of $\Omega = 90°$, the pressure drop for the tube of $6\ mm$ is $97\ mbar/m$, while for $4\ mm$ is $136\ mbar/m$, i.e., 40.5% higher. Instead, for $8\ mm$ is $91\ mbar/m$, only a 5.7% lower than the case of $6\ mm$.

For the case of oriented tubes ($\Omega > 0°$), only for the case of $D = 4\ mm$, the pressure drop is higher for two-phase flow than that for liquid flow. The reason is that, for 6 and $8\ mm$, the head gravitational effect is more significative than the frictional effect.

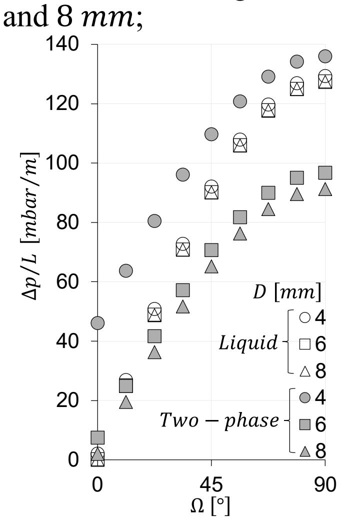

Figure 3. Pressure drop per length unit as function of D and Ω.

Figure 4 depicts the contribution of the frictional pressure drop on the total pressure drop, $\Delta p_f/\Delta p$, for different inner tube diameter, D, due to the tube orientation, Ω.

For horizontal tubes ($\Omega = 0°$), the total pressure drop is comprised entirely of frictional losses, as the gravitational head effect is absent.

For the case of oriented tubes ($\Omega > 0°$), only the case of $D = 4\ mm$, for two-phase flow, shows a significative effect of frictional pressure drop, being 42.6% and 34.5% for $45°$ and $90°$, respectively.

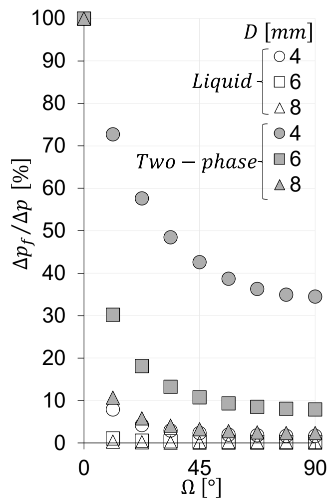

Figure 4. Contribution of frictional pressure drop to total pressure drop as function of D and Ω.

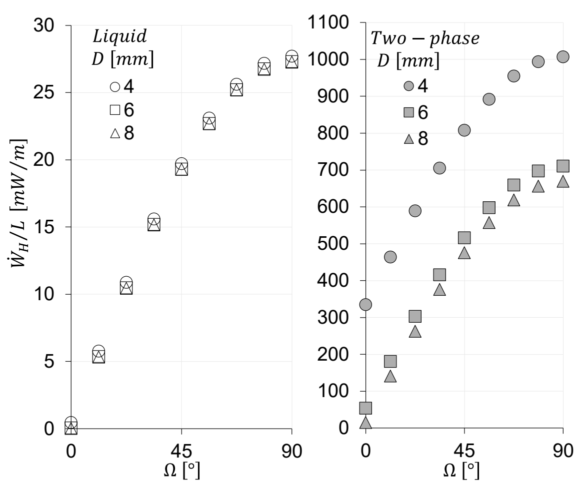

Figure 5. Hydraulic power per length unit as function of D and Ω.

Figure 5 depicts the effect of the tube orientation, Ω, on the hydraulic power per unit of length, $\dot{W}_H/L$, for different inner tube diameter, D. The liquid flow and the two-phase flow are shown in different graphs in order to observe differences due to the scales.

The left figure is for liquid flow, while the right one is for two-phase flow. Note the different scale of the ordinate-axis in both figures.

For the case of liquid flow, the effect of the inner tube diameter is almost negligible; while for the case of two-phase flow, such effect is considerable; for example, the hydraulic power for $D = 4\,mm$ is 520.2%, 56.6%, and 41.8% higher than for $D = 6\,mm$, for $\Omega = 0°, 45°,$ and $90°$, respectively. The hydraulic power, for $D = 6\,mm$ is 260.6%, 8.5%, and 6.2% higher than for $D = 8\,mm$, respectively.

Figure 6 depicts the effect of the tube orientation, Ω, on the rate of entropy production per unit of length, $\dot{\sigma}/L$, for different inner tube diameter, D. The liquid flow and the two-phase flow are shown in different graphs to observe differences due to the scales.

The left figure is for liquid flow, while the right one is for two-phase flow. Note the different scale of the ordinate-axis in both figures.

The inner tube diameter plays and important effect due to the entropy production is product of the frictional effect. The tube orientation has negligible effect on the entropy production. By comparison, for two-phase flow and $\Omega = 0°$, the entropy production for $D = 4\,mm$ is 600.8% higher than that for $D = 6\,mm$; while the entropy production for $D = 6\,mm$ is 293.2% higher than that for $D = 8\,mm$.

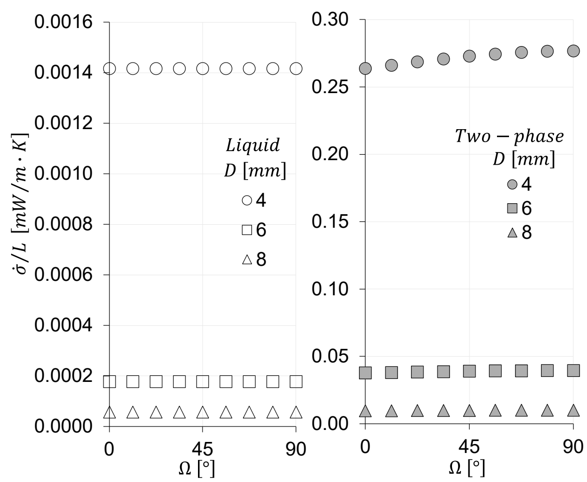

Figure 6. Rate of entropy production per length unit as function of D and Ω.

Figure 7 depicts the effect of the tube orientation, Ω, on the outlet temperature, T_{out}, for different inner tube diameter, D. The liquid flow and the two-phase flow are shown in different graphs to observe differences due to the scales.

The left figure is for liquid flow, while the right one is for two-phase flow. Note the different scale of the ordinate-axis in both figures.

The temperature is function of the pressure, so the higher pressure drop the higher temperature difference between the inlet and the outlet. In effect, the vertical tube ($\Omega = 90°$) shows the higher temperature difference. Also, because the smaller the tube diameter the higher the pressure drop, the case of $D = 4\,mm$ presents the highest temperature difference. For liquid flow, there is almost no effect of inner tube diameter on the outlet temperature.

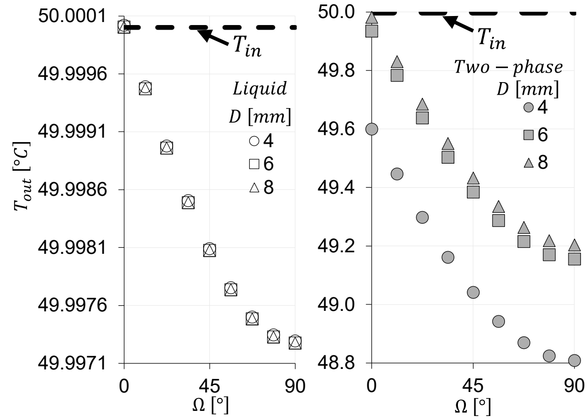

Figure 7. Outlet temperature as function of D and Ω.

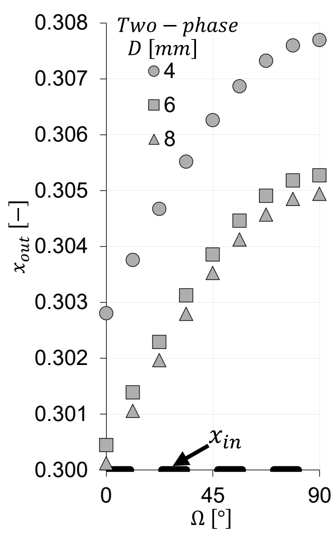

Figure 8. Outlet mass quality as function of D and Ω.

Table 4. Requirements to minimize the main design parameters.

To minimize	Increase or decrease	
	D	Ω
$\dot{W}_H$	↑	↓
$\dot{\sigma}$	↑	-
$\Delta T = \lvert T_{in} - T_{out} \rvert$	↑	↓
$\Delta x = \lvert x_{in} - x_{out} \rvert$	↑	↓

Figure 8 depicts the effect of the tube orientation, Ω, on the outlet mass quality, x_{out}, for different inner tube diameter, D.

As the case of outlet temperature, the quality is function of the pressure, so the higher pressure drop the higher quality difference between the inlet and the outlet. In effect, the vertical tube ($\Omega = 90°$) shows the higher quality difference. Also, because the smaller the tube diameter the higher the pressure drop, the case of $D = 4\,mm$ presents the highest quality difference. Table 4 summarizes the requirements for minimizing key design parameters. Peak piping performance can be achieved using the biggest inner tube diameter and the lowest tube slope.

4. Conclusions

This paper presents an own algorithm that, based on a one-dimensional steady-state model, permits to compute key parameters of a single oriented mini-tube for electronic cooling. A comprehensive parametric analysis, utilizing a single oriented tube with R1336mzz(Z) as the working fluid, is presented as example of the use of such algorithm.

The most significant findings from the simulated parameter range are as follows:

- The minimum hydraulic pumping power is achieved with the biggest inner tube diameter, and/or the lowest tube slope.
- The minimum rate of entropy production is achieved at the biggest inner tube diameter, while the tube orientation has no effect.
- The minimum temperature and mass quality differences, between the tube inlet and outlet, are achieved with the biggest inner tube diameter, and/or the lowest tube slope.

In conclusion, for the design parameters here analyzed, the peak performance for the pipes is achieved with the biggest inner tube diameter, and/or the lowest tube slope.

Acknowledgments

The authors would like to extend their sincere gratitude to "In Quattro" for the funding to carry out the research stay for the development of this project.

References

[1] Tibirica CB, Ribatski G. (2013). Flow boiling in micro-scale channels - Synthesized literature review. "International Journal of Refrigeration", 36(2), 301-324.
[2] Saisorn S, Wongwises S. (2008). A review of two-phase gas-liquid adiabatic flow characteristics in micro-channels. "Renewable and Sustainable Energy Reviews", 12(3), 824-838.
[3] Xu Y, Fang X, Su X, Zhou Z, Chen W. (2012). Evaluation of frictional pressure drop correlations for two-phase flow in pipes. "Nuclear Engineering and Design", 253, 86-97.
[4] Santra S, Mandal S, Chakraborty S. (2020). Phase-field modeling of multicomponent and multiphase flows in microfluidic systems: a review. "International Journal of Numerical Methods for Heat & Fluid Flow", 31(10), 3089–3131.
[5] Wörner M. (2012). Numerical modeling of multiphase flows in microfluidics and micro process engineering: a review of methods and applications. "Microfluid Nanofluid", 12, 841-886.
[6] Xiao JJ, Shonham O, Brill JP. (1990). A comprehensive mechanistic model for two-phase flow in pipelines. "SPE Annual Technical Conference and Exhibition".
[7] Parlak N, Gür M, Ari V, Küçük H, Engin T. (2011). Second law analysis of water flow through smooth microtubes under adiabatic conditions. "Experimental Thermal and Fluid Science", 35(1).
[8] Celata GP, Cumo M, Marconi V, McPhail SJ, Zummo G. (2006). Microtube liquid single-phase heat transfer in laminar flow. "International Journal of Heat and Mass Transfer", 49(19-20), 3538-3546.
[9] Zhuo L, He YL, Tang GH, Tao WQ. (2007). Experimental and numerical studies of liquid flow

and heat transfer in microtubes. “International Journal of Heat and Mass Transfer”, 50(17-18), 3447-3460.
[10] Sahar AM, Wissink JG, Mahmoud MM, Ishak MSA, Karayiannis TG. (2021). Numerical study of two-phase flow in vertical microtubes: Adiabatic flow pattern maps. “7th Micro and Nano Flows Conference”.
[11] Ghorai S, Nigam KDP. (2006). CFD modeling of flow profiles and interfacial phenomena in two-phase flow in pipes. “Chemical Engineering and Processing: Process Intensification”, 45(1), 55-65.
[12] Koo J, Kleinstreuer C. (2004). Viscous dissipation effects in microtubes and microchannels. “International Journal of Heat and Mass Transfer”, 47(14-16), 3159-3169.
[13] Chinnov EA, Kabov OA. (2006). Two-phase flows in pipes and capillary channels. “High Temperature”, 44, 773-791.
[14] Brauner N, Ullmann A. (2023). Modelling of flow pattern transitions in small diameter horizontal and inclined tubes. “Experimental Thermal and Fluid Science”, 148, 110965.
[15] Van Rossum G. (2023). Python Manual. Python Software V. 3.11.1
[16] Shah RK, London AL. (2014). Laminar flow forced convection in ducts: a source book for compact heat exchanger analytical data. Academic press.
[17] Phillips RJ. (1987). Forced convection, liquid cooled, microchannel heat sinks. MS Thesis, Department of Mechanical Engineering, Massachusetts Institute of Technology, Cambridge, MA.
[18] Bejan A. (1996). Entropy generation minimization: The new thermodynamics of finite-size devices and finite-time processes. “Journal of Applied Physics”, 79, 1191-1218.
[19] Carey VP. (1992). Liquid-vapor phase change. Taylor & Francis.
[20] Lockhart RW, Martinelli RC. (1949). Proposed correlation of data for isothermal two-phase, two-component flow in pipes. “Chemical Engineering Progress”, 45(1), 38-48.
[21] https://w-refrigerant.com/en/latest_refrigerant-en/r1336mzzz/
[22] Huber M, Harvey A, Lemmon E, Hardin G, Bell I, McLinden M. (2018). NIST Reference Fluid Thermodynamic and Transport Properties Database (REFPROP) Version, 9.1